Applied Physics Letters

Size-derived reaction mechanism of core-shell aluminum nanoparticle

Cite as: Appl. Phys. Lett. **117**, 133902 (2020); https://doi.org/10.1063/5.0015367
Submitted: 27 May 2020 . Accepted: 08 September 2020 . Published Online: 29 September 2020

Qingzhao Chu, Baolu Shi, Lijuan Liao, Yintao Zhou, Kai H. Luo, and Ningfei Wang

Applied Physics Letters ARTICLE scitation.org/journal/apl

Size-derived reaction mechanism of core-shell aluminum nanoparticle

Cite as: Appl. Phys. Lett. **117**, 133902 (2020); doi: 10.1063/5.0015367
Submitted: 27 May 2020 · Accepted: 8 September 2020 ·
Published Online: 29 September 2020

Qingzhao Chu,[1] Baolu Shi,[1,a)] Lijuan Liao,[2,a)] Yintao Zhou,[1] Kai H. Luo,[3] and Ningfei Wang[1]

AFFILIATIONS

[1]School of Aerospace Engineering, Beijing Institute of Technology, No. 5 ZhongGuanCun South Street, Haidian, Beijing 100081, China
[2]Institute of Mechanics, Chinese Academy of Sciences, No. 15 BeiSihuan West Road, Beijing 100190, China
[3]Department of Mechanical Engineering, University College London, Torrington Place, London WC1E 7JE, United Kingdom

[a)]**Authors to whom correspondence should be addressed:** shibaolu@bit.edu.cn and smashingsky@hotmail.com. **Tel:** +86-10-6891-3623 and liaohuanxin@hotmail.com. **Tel:** +86-10-8254-4291

ABSTRACT

To prompt the application of aluminum nanoparticles (ANPs) in combustion as the fuel additive and in chemical synthesis as the catalyst, this study examines the reaction dynamics of core-shell ANPs under an oxygen atmosphere via Transient Non-Equilibrium Reactive Molecular Dynamics simulations. Two distinct oxidation modes determined by the competition between the oxide shell melting and core reaction have been identified. One is the fast oxidation mode with a high reaction heat release rate, where core Al and ambient O atoms diffuse into each other to form a homogeneous alumina particle. The other is the moderate oxidation with lower heat release, where only core Al atoms diffuse into the oxide shell to form a hollow spherical structure. By modeling the shell melting and Al core reaction, a size-derived oxidation model has been proposed to conveniently but accurately predict the ANP reaction dynamics. This work also provides fundamental insight into the synthesis of ANPs that serve as a high energy density fuel and high-performance catalyst.

Aluminum nanoparticles (ANPs) are recognized as attractive fuel additives in energetic materials like propellants and explosives,[1] owing to the merits of high energy density, low cost, and safety.[2] Meanwhile, ANPs with a hollow structure have drawn extensive attention in the catalysis,[3,4] energy storage,[5] and biomedical areas.[6] Understanding the reaction mechanism is of vital importance for the application of ANPs, e.g., improvement of metal fuel combustion efficiency and manipulation of the surface to volume ratio and internal void morphology of hollow metal particles.[7] The reaction behaviors of ANPs are generally assumed to be dominated by the particle radius (R). For example, Rai *et al.*[8] examined the size dependent reactivity and provided a power law relation between oxidation time and R. A melt-dispersion theory was then proposed by Levitas *et al.*[9] They argued that the ratio of the core radius to oxide shell thickness was the key factor controlling ANP reaction rather than the whole particle radius. In the molecular dynamics (MD) simulation, Li *et al.*[10] observed that the reaction behaviors were the same for ANPs with a diameter of 26–46 nm, and the reaction rate accelerated as the ANP size decreased. In the reaction of a smaller size ANP (core radius: 3 nm; oxide thickness: 1 nm), Chu *et al.*[11] reported that the reaction initiated from the core-shell interface, and the core Al atoms and shell O atoms diffused into each other. While in another MD simulation (core radius of 5 nm; shell thickness of 2 and 4 nm), Wu *et al.*[12] reported the formation of hollow structures, which is probably attributed to the one-direction diffusion of the core atom to the shell. The aforementioned results illustrate the size-dependent transition of reaction behaviors. By employing MD simulation, this study provides a clear understanding of the underlying atomic process and proposes a convenient and effective method to predict the ANP reaction dynamics according to its initial configuration.

To examine the size effect on the ANP reaction dynamics, Transient Non-Equilibrium Reactive Molecular Dynamics (TNE-RMD)[13,14] is performed using the LAMMPS package.[15] ReaxFF Force-Field[16,17] is applied to describe the interactions for the ANP and oxygen, and more detailed information about developments and applications of ReaxFF has been summarized in depth in the literature.[18] There are numerous experimental literature studies on the oxidation of ANPs including tens of nanometers in diameter for energetics[9,19,20] and a few nanometers for catalysis.[21–23] Recently, the size range of 1–10 nm has received keen interest in ANP oxidation,[12,24–27] where the shell thickness lies in the range of experimental conditions (1–4 nm).[9,20]

In this Letter, ANPs with a diameter of 4–14 nm are investigated to examine the size effect on ANP oxidation behaviors. A series of core-shell ANPs under an oxygen atmosphere are constructed with different geometric parameters, where the core radiuses (C) are in the range of 1.5–5.0 nm and the oxide shell thicknesses (S) are between 0.5 and 2.0 nm. These cases are denoted as "C*S*." To maintain the same ambient pressure of 20 MPa, the numbers of oxygen molecules and box sizes are varied according to the specific ANP size. Finally, TNE-RMD is performed by relaxing ANP under the NVE ensemble while thermalizing the oxygen molecules at 2000 K under NVT ensemble for up to 600 ps. More details are listed in the supplementary material.

Two different reaction modes are identified for these ANPs, i.e., the fast oxidation (Fast-Ox) and moderate oxidation (Moderate-Ox). Three cases of C2S1, C2S2, and C5S2 are selected to illustrate the differences. Snapshots of ANPs at representative stages of initial, ignition, and end of simulation are listed in Fig. 1(a). When the consumption rate of core Al atoms reaches its maximum, the ANP ignition is assumed to occur.[11] The initial structures present the fcc-Al core and amorphous oxide shell. After ignition, cases C2S1 and C5S2 experience fast oxidation, where the core Al atoms react intensely with the oxide shell and ambient oxygen, turning into an almost homogeneous alumina particle at the end. For the case of C2S2, asymmetrical voids are observed around ignition, and the final structure becomes a hollow alumina shell. Ambient oxygen molecules are absorbed at the shell without entering the core to react with Al atoms. The observed hollow structure is similar to that described in Ref. 12. The hollow structures have also been found in experiments of ANP[28] and Ni–Fe bimetallic nanoparticles,[29] which further validate our observation. It is seen that as the S increases (e.g., C2S1–C2S2), the reaction mode may convert from Fast-Ox to Moderate-Ox; as C increases (e.g., C2S2 to C5S2), the reaction mode turns to Fast-Ox inversely.

The different reaction modes are assumed to be induced by the specific physical and chemical properties of the ANP. Hence, detailed evolution of the ANP micro-structure is examined in Fig. 1(b). According to Ref. 11, $MSD_{10000} > 0.5$ Å is adopted to predict the melting of the Al core and oxide shell. For C2S1 and C5S2, both the core and oxide are totally melted before the onset of ignition. The core Al and ambient O atoms diffuse into each other after ignition. For C2S2

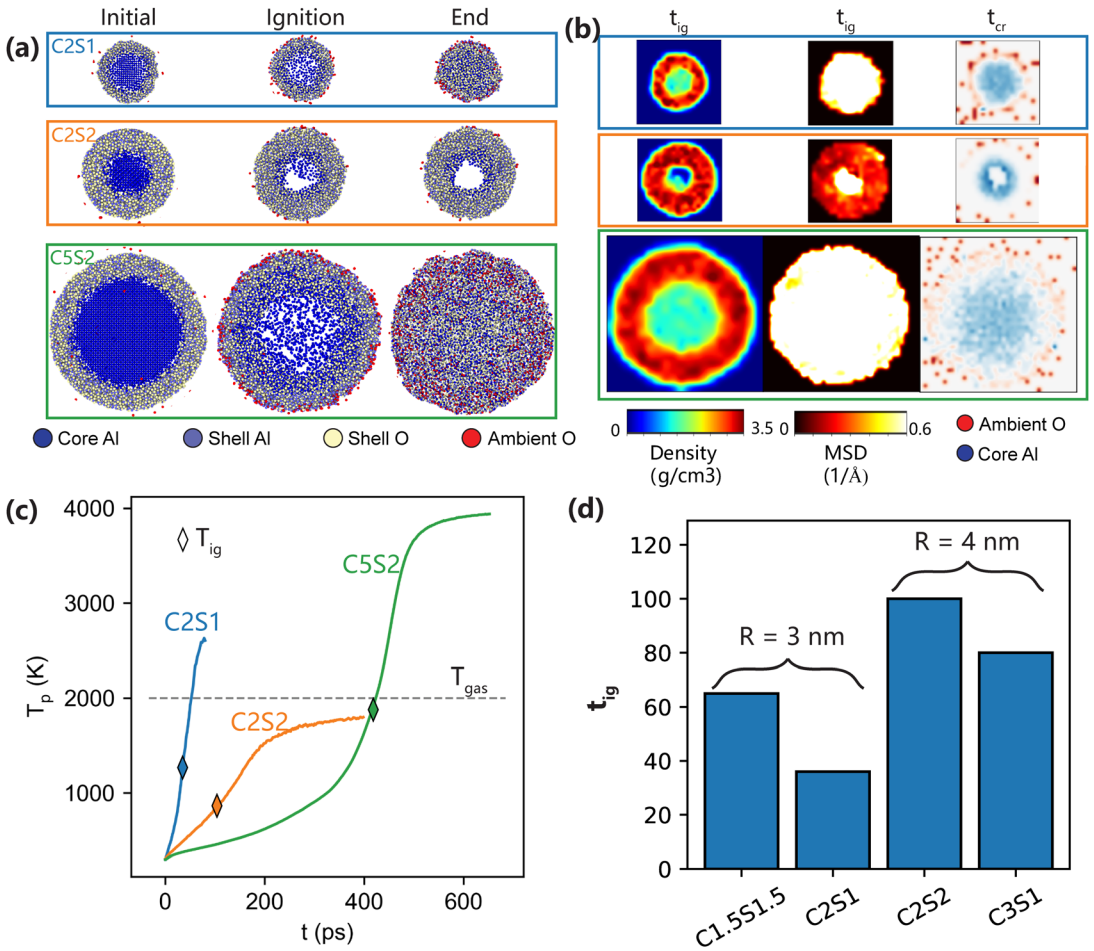

FIG. 1. (a) Snapshots of ANPs at the instants of initial, ignition, and end of simulation, (b) distribution of density and $MSD_{10\,000}$ at ignition and atomic distribution around core run out, (c) temporal variations of ANP temperature, and (d) ignition delay time for ANPs with $R = 3$ and 4 nm.

(Moderate-Ox), only the core is melted at the instant of ignition, and the final structure indicates that core Al and ambient O atoms are separated from each other.

Temporal variations of average ANP temperature (T_p) are also examined [Fig. 1(c)] to demonstrate the reaction characteristics. For both C2S1 and C5S2 (Fast-Ox), after ignition, T_p rises significantly and the final temperatures are higher than ambient temperature (T_{gas}). While for C2S2, the particle temperature at ignition (T_{ig}) is much low, indicating that the particle may not be truly ignited. The temperature increase is much limited after ignition.

The reaction rates of ANPs with the same R but different C and S are discussed via the ignition delay times (t_{ig}) defined as the duration from the beginning to the onset of ignition [Fig. 1(d)]. For ANPs with $R = 3$ nm, C1.5S1.5 yields a larger t_{ig} than C2S1. With increasing S, t_{ig} also increases in the cases of $R = 4$ nm. The result contradicts with the reported ANP oxidation theory,[8] indicating that it is C and S rather than the whole particle radius that dominate the reaction dynamics.

Based on Fig. 1(b), the melting of the oxide shell seems to play a key role in determining the reaction mode, as the phase transition affects the atomic diffusivity and reaction rate, which leads to different heat release rates and final product. The melting temperature is determined by evaluating the Gibbs free energy of nanostructures in solid and liquid phases. Here, three kinds of models are employed to analyze the melting point of oxide (T_m) in the core-shell ANP, where the major difference lies in the calculation of Gibbs free energy. As shown in Fig. 2(a), Model I adopts an infinite planar film to analogy the spherical shell,[30]

$$T_{m,I} = T_0\left(1 - \left(\frac{A_o + A_i}{V}\right)\frac{(\gamma_{s,f} - \gamma_{l,f})}{\rho_s \Delta H_{m,ox}}\right), \quad (1)$$

where T_0 is the bulk melting point of alumina, A_o and A_i denote the outer and inner surface areas of the oxide shell, ρ_s is the solid phase density, $\Delta H_{m,ox}$ is the latent heat of oxide melting, and $(\gamma_{s,f} - \gamma_{l,f})$ denotes the surface free energy difference between solid and liquid phases. The detailed formula derivations are listed in the supplementary material.

Model II is a single free surface model proposed by Joshi *et al.*[31] They argued that the inner surface is strictly not a free surface, and by ignoring the inner surface, it is obtained that

$$T_{m,II} = T_0\left(1 - \frac{A_o(\gamma_{s,f} - \gamma_{l,f})}{V\rho_s \Delta H_{m,ox}}\right). \quad (2)$$

The predicted T_m values by models I and II are compared with the MD simulations [Fig. 2(b)]. The thermalized C_{eq} and S_{eq} (listed in Table S1) are adopted in Eqs. (1) and (2) to predict T_m. Model I yields a lower T_m for thin oxide. For example, the predicted value for C1.5S0.5 is about 600 K lower than the MD result. However, Model II overestimates T_m for ANPs with $S \geq 1$ nm. These discrepancies are attributed to inappropriate treatment with the core-shell interface. Here, another method denoted as Model III has been constructed, which introduces an interface energy difference term $(\gamma_{s,i} - \gamma_{l,i})$ to improve accuracy,

$$T_{m,III} = T_o\left(1 - \frac{A_o(\gamma_{s,f} - \gamma_{l,f}) + A_i(\gamma_{s,i} - \gamma_{l,i})}{V\rho_s \Delta H_{m,ox}}\right), \quad (3)$$

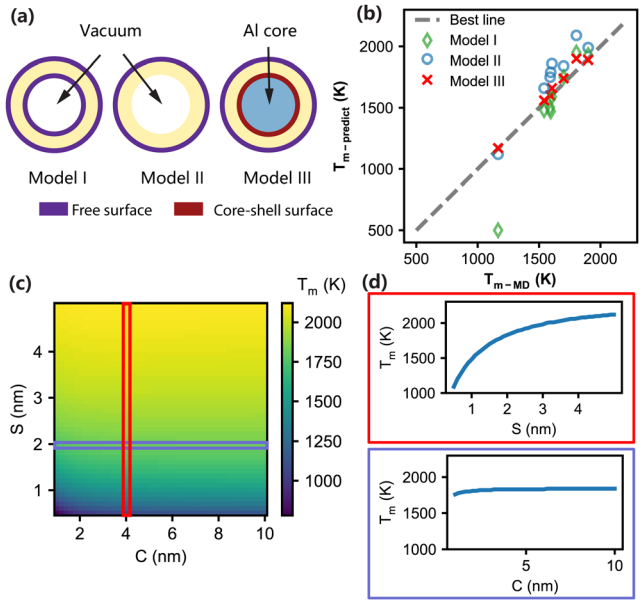

FIG. 2. (a) Illustrations of three melting models. The purple and red curves represent the free surface and core–shell interface, respectively, and (b) melting points of the oxide shell calculated by MD and three melting models. The dashed line represents the best prediction line. (c) Contour of the predicted shell melting points based on model III in the S–C coordinate. (d) Variations of the shell melting point with the shell thickness ($C = 4$ nm, red rectangular box in (c)) and core radius [$S = 2$ nm, purple rectangular box in (c)].

where $\gamma_{s,i}$ and $\gamma_{l,i}$ represent the core-shell interface energy at solid phase and liquid phases, respectively. The values of interface free energy are fitted through MD simulations. As indicated in Fig. 2(b), the predictions by Model III show good agreement with the MD results over different shell thicknesses. By introducing an interface energy term, our model corrected the discrepancy to less than 100 K, which is in contrast to ~600 K of Model I and ~350 K of Model II. The contour of T_m predicted by Model III is shown in Fig. 2(c), where C varies from 1 to 10 nm and S increases from 0.5 to 5 nm. As R increases, T_m increases from 800 to 2300 K, which is close to the bulk melting point of alumina (2327 K).[32] It seems that T_m is insensitive to C but strongly dependent on S. Hence, the specific variations of T_m with C and S are discussed in Fig. 2(d). For the ANP with $C = 4$ nm, T_m increases from 1100 K to 2200 K as S increases from 0.5 to 5 nm. As the shell melts, the diffusivity of oxygen atoms in the oxide shell is enhanced, resulting in the rapid increase in the ANP oxidation rate and fierce heat release. Such an increment is often regarded as the ignition of the ANP, and so the melting temperature of the oxide shell is also defined as the ANP ignition temperature in this Letter. Recently, it is reported that the ignition temperatures increase from 1000 to 2300 K as the ANP size in the range of 10 nm to 10 μm,[20] and there has not been a reasonable explanation for the transition of ignition temperature. We found that the experimental ignition temperature range agrees well with those predicted by our theoretical models. Hence, it is reasonable to conclude that the ANP ignition is significantly affected by the size-dependent melting of the oxide shell, which is determined by the core radius and shell thickness.

After determining T_m, the main question is whether T_p could reach T_m through both reaction heat release (Q_{reax}) and heat transfer (Q_{trans}). According to Ref. 25, Q_{reax} and Q_{trans} are calculated. The contribution of Q_{reax} is quantified by $q_r = Q_{reax}/(Q_{reax}+Q_{trans})$. Figure 3(a) shows q_r at the instant of Al core run out, until which most of reaction heat has been released. For Fast-Ox, q_r is larger than 1, suggesting a negative value of Q_{trans}. That is to say, the heat transfer direction changes from the ANP to the environment. For case C2S2, q_r is close to 0.8. For other cases, the contribution of heat transfer is lower than 20%, which generally becomes much weak as the particle temperature increases. To simplify the calculation, only Q_{reax} is adopted to calculate the temperature increment until core run out. Thus, the ANP temperature at the instant of core run out (T_{cr}) is calculated as

$$T_{cr} = T_{init} + \frac{\Delta H_r dn_{Al} - \Delta H_{m,c} m_c}{c_s m_s + c_c m_c}, \quad (4)$$

where T_{init} is the initial ANP temperature, ΔH_r is the reaction enthalpy, $\Delta H_{m,c}$ is the latent heat of core melting, m_s and m_c are the mass of the initial shell and core, respectively, and c_s and c_c are the specific heat of alumina and Al, respectively.

As shown in Fig. 3(b), the predicted T_{cr} (○) agrees well with the MD result in Moderate-Ox. For Fast-Ox, Eq. (4) overestimates T_{cr} (▼) because of ignoring the heat transfer effect. By simply counting the heat loss through heat transfer between the ANP (assuming $T_p = T_{cr}$) and environment (T_{gas}), a modified T_{cr}^* (▽) can be obtained, which coincides very well with MD simulation.

Finally, the models of shell melting [Eq. (3)] and reaction heat release [Eq. (4)]) are employed to quantitatively predict the reaction mode. The boundary between fast and moderate modes is determined by T_{cr} and T_m, which are first calculated by the ANP geometry and environmental conditions. If $T_m > T_{cr}$, where the particle temperature at the instant of core run out is lower than the melting point of oxide shell, the reaction mode is Moderate-Ox. It indicates that the ANP reaction heat is insufficient to melt the oxide shell and the reaction is moderate, yielding a hollow structure. However, if $T_m \le T_{cr}$, the oxidation mode is Fast-Ox. The MD results are also mapped in Fig. 4 for validation (× for Fast-Ox and ○ for Moderate-Ox), confirming that the current theoretical model can well predict the reaction mode. The boundary between the two modes can be plotted with a linear fit of $S = 1.03C + 0.4$ (dashed line). The modified T_{cr}^* improves the prediction for ANPs with large C and S, as indicated by the grey band along the boundary.

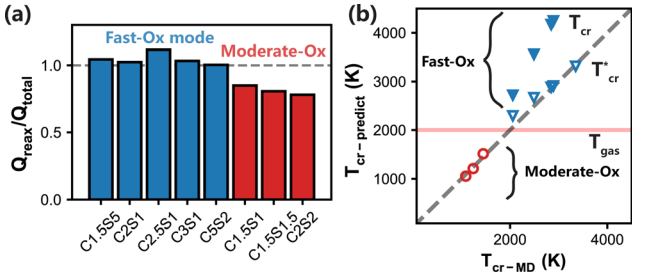

FIG. 3. (a) Contribution of reaction heat release to ANP heating for Fast-Ox (blue column) and Moderate-Ox mode (red) and (b) comparison between T_{cr} (T_{cr}^*) calculated by Eq. (4) and MD.

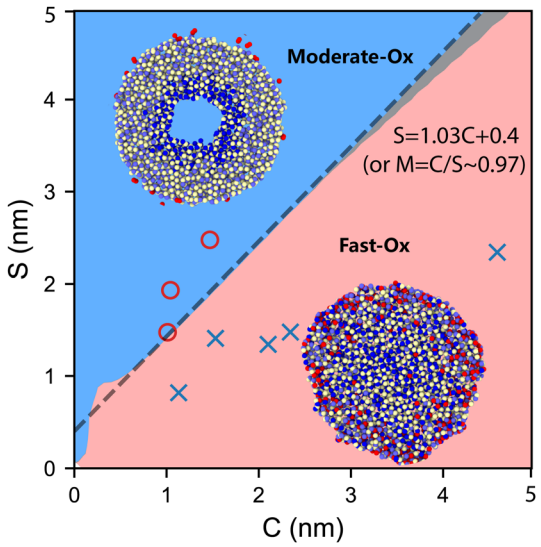

FIG. 4. Phase diagram of the reaction modes based on the proposed model. Fast-Ox and Moderate-Ox modes are marked by × and ○ for MD simulations.

As R increases, the boundary between the two modes approaches $M = C/S = 0.97$. Since S generally lies in $1 < S < 5$ nm, the reaction mode for ANPs with $C > 5$ nm is dominated by the Fast-Ox. Previous studies mainly focus on the size of aluminum core, and the effects of the oxide shell are less concerned. However, the present model shows that the oxidation dynamics of the ANP is determined by the competition between core ignition and oxide shell melting. Moreover, the transition of ignition temperature in experiments also validates the dominant role of core ignition/shell melting competition.[20] Thus, we believe that the current theoretical model is applicable to estimate the oxidation behaviors of larger ANPs.

In summary, the reaction dynamics of ANPs with different core and shell sizes has been investigated via TNE-RMD simulations. Two reaction modes of fast and moderate oxidation are observed, which yield homogeneous and hollow structures, respectively. The reaction mode is determined by the competition between the oxide shell melting and Al core reaction. Based on the ANP configuration, two models are constructed to predict the oxide melting point and estimate the heat release of the core Al reaction. A size-derived model has been proposed, which provides a convenient but accurate method to predict the reaction dynamics of ANPs based on its initial geometry, i.e., core radius and shell thickness. By tuning the shell thickness and core radius, which directly relate to the shell melting and exothermic reaction, the transition between weak- and intense-exothermic oxidation can be achieved. The proposed model reveals the oxidation mechanism derived from the initial particle configuration, providing a guideline for the synthesis of high-performance metal fuels and catalysts.

See the supplementary material for the detailed description of ANP configurations and MD simulation settings and theoretical models of shell melting and core oxidation.

This work was supported by the Equipment Advance Research Field Foundation (Grant No. 61407200201) and National Natural

Science Foundation of China (Grant Nos. 11672314 and 51676016). The computations were supported by the Computing Facility, Institute of Mechanics, Chinese Academy of Sciences, and Tianhe-2 National Supercomputer Center in Guangzhou.

DATA AVAILABILITY

The data that support the findings of this study are available from the corresponding author upon reasonable request.

REFERENCES

[1]S. A. Davari, J. L. Gottfried, C. Liu, E. L. Ribeiro, G. Duscher, and D. Mukherjee, Appl. Surf. Sci. **473**, 156 (2019).
[2]D. Sundaram, V. Yang, and R. A. Yetter, Prog. Energy Combust. Sci. **61**, 293 (2017).
[3]Q. Cui, Y. Sha, J. Chen, and Z. Gu, J. Nanopart. Res. **13**, 4785 (2011).
[4]G. Prieto, H. Tüysüz, N. Duyckaerts, J. Knossalla, G.-H. Wang, and F. Schüth, Chem. Rev. **116**, 14056 (2016).
[5]J. Wang, Y. Cui, and D. Wang, Adv. Mater. **31**, 1801993 (2019).
[6]S.-F. Lee, X.-M. Zhu, Y.-X. J. Wang, S.-H. Xuan, Q. You, W.-H. Chan, C.-H. Wong, F. Wang, J. C. Yu, C. H. K. Cheng, and K. C.-F. Leung, ACS Appl. Mater. Interfaces **5**, 1566 (2013).
[7]J. G. Railsback, A. C. Johnston-Peck, J. Wang, and J. B. Tracy, ACS Nano **4**, 1913 (2010).
[8]A. Rai, K. Park, L. Zhou, and M. R. Zachariah, Combust. Theory Modell. **10**, 843 (2006).
[9]V. I. Levitas, M. L. Pantoya, and B. Dikici, Appl. Phys. Lett. **92**, 011921 (2008).
[10]Y. Li, R. K. Kalia, A. Nakano, and P. Vashishta, J. Appl. Phys. **114**, 134312 (2013).
[11]Q. Chu, B. Shi, L. Liao, K. H. Luo, N. Wang, and C. Huang, J. Phys. Chem. C **122**, 29620 (2018).
[12]B. Wu, F. Wu, Y. Zhu, A. He, P. Wang, and H. Wu, J. Appl. Phys. **126**, 144305 (2019).
[13]A. Rajabpour, R. Seif, S. Arabha, M. M. Heyhat, S. Merabia, and A. Hassanali, J. Chem. Phys. **150**, 114701 (2019).
[14]R. Meland, J. Chem. Phys. **117**, 7254 (2002).
[15]S. Plimpton, J. Comput. Phys. **117**, 1 (1995).
[16]S. Hong and A. C. T. van Duin, J. Phys. Chem. C **119**, 17876 (2015).
[17]S. Hong and A. C. T. van Duin, J. Phys. Chem. C **120**, 9464 (2016).
[18]T. P. Senftle, S. Hong, M. M. Islam, S. B. Kylasa, Y. Zheng, Y. K. Shin, C. Junkermeier, R. Engel-Herbert, M. J. Janik, and H. M. Aktulga *et al.*, Npj Comput. Mater. **2**(1), 15011 (2016).
[19]G. A. Risha, S. F. Son, R. A. Yetter, V. Yang, and B. C. Tappan, Proc. Combust. Inst. **31**, 2029 (2007).
[20]D. S. Sundaram, P. Puri, and V. Yang, Combust. Flame **169**, 94 (2016).
[21]A. C. Reber, S. N. Khanna, P. J. Roach, W. H. Woodward, and A. W. Castleman, J. Am. Chem. Soc. **129**, 16098 (2007).
[22]W. H. Woodward, N. Eyet, N. S. Shuman, J. C. Smith, A. A. Viggiano, and A. W. Castleman, J. Phys. Chem. C **115**, 9903 (2011).
[23]Z. Luo, A. W. Castleman, and S. N. Khanna, Chem. Rev. **116**, 14456 (2016).
[24]Y. R. Zhang, A. C. T. van Duin, and K. H. Luo, Fuel **234**, 94 (2018).
[25]Q. Chu, B. Shi, L. Liao, X. Zou, K. H. Luo, and N. Wang, J. Phys. Chem. C **124**, 3886 (2020).
[26]G. Li, L. Niu, W. Hao, Y. Liu, and C. Zhang, Combust. Flame **214**, 238 (2020).
[27]X. Zhang, C. Fu, Y. Xia, Y. Duan, Y. Li, Z. Wang, Y. Jiang, and H. Li, ACS Nano **13**, 3005 (2019).
[28]G. Viau, V. Collière, L.-M. Lacroix, and G. A. Shafeev, Chem. Phys. Lett. **501**, 419 (2011).
[29]W. Xia, Y. Yang, Q. Meng, Z. Deng, M. Gong, J. Wang, D. Wang, Y. Zhu, L. Sun, F. Xu, J. Li, and H. L. Xin, ACS Nano **12**, 7866 (2018).
[30]G. Guisbiers and L. Buchaillot, J. Phys. Chem. C **113**, 3566 (2009).
[31]N. Joshi, N. Mathur, T. Mane, and D. Sundaram, Comput. Mater. Sci. **145**, 140 (2018).
[32]D. R. Stull and H. Prophet, *National Standard Reference Data System. JANAF Thermochemical Tables* (US Dept. of Commerce, National Bureau of Standards, Washington, 1971).